ADVANCED FUNCTIONAL MATERIALS
www.afm-journal.de

Deterministic Current-Induced Perpendicular Switching in Epitaxial Co/Pt Layers without an External Field

*Jeongchun Ryu, Can Onur Avci, Moojune Song, Mantao Huang, Ryan Thompson, Jiseok Yang, San Ko, Shutaro Karube, Nobuki Tezuka, Makoto Kohda, Kab-Jin Kim, Geoffrey S. D. Beach, and Junsaku Nitta**

Current-induced spin-orbit torques (SOTs) have emerged as a powerful tool to control magnetic elements and non-uniform magnetic textures such as domain walls and skyrmions. SOT-induced switching of perpendicular magnetization generally requires an external field to break the rotational symmetry of the spin-orbit effective fields responsible for the deterministic reversal. The proposed mechanisms to eliminate this requirement often rely on complex multilayer structures that necessitate laborious optimization in the material and spin transport properties, making them less attractive for applications. Herein, current-induced, external field-free switching of an epitaxial MgO/Pt/Co trilayer with an extremely large perpendicular anisotropy in excess of 3 Tesla is reported. It is found that switching occurs due to the interplay of strong SOTs, local anisotropy fluctuations, and the Dzyaloshinkii-Moriya interaction inherent to this epitaxial system. Given that these layers constitute the base stack of a magnetic tunnel junction, this switching mechanism offers the most technologically viable path toward devices such as field-free SOT-based magnetic random-access memories.

1. Introduction

Spin orbit torques (SOTs) driven by the spin Hall and interfacial spin galvanic effects have been extensively studied and utilized to control the magnetization in ferromagnet/normal metal (FM/NM) heterostructures.[1–10] In such a mechanism, a charge current flowing through the layers exerts a field-like (FL-SOT) and a damping-like (DL-SOT) torque, with symmetries $\boldsymbol{\tau}_{FL} = \mathbf{m} \times \mathbf{y}$ and $\boldsymbol{\tau}_{DL} = \mathbf{m} \times (\mathbf{m} \times \mathbf{y})$ (here $\mathbf{y}$ is the in-plane axis transverse to the current flow, $\mathbf{z}$ is the out-of-plane direction), respectively, independent of the interactions from which they originate. SOTs have a symmetry suitable to switch in-plane magnetization pointing transverse to the current injection axis through an anti-damping process facilitated by thermal fluctuations, without requiring an external field.[2,11] This mechanism is analogous to conventional spin-transfer torque switching in spin valves or magnetic tunnel junctions (MTJ),[12,13] where the spin polarized current is substituted by the pure spin current generated by bulk and interfacial spin-orbit coupling.[2,11,14–17]

Devices based on in-plane magnetization switching have some inherent drawbacks related to, e.g., limitations in device shape and size due to the requirement of large in-plane anisotropies and longer switching times due to slow incubation.[18] FMs with perpendicular magnetic anisotropy (PMA), on the other hand, are far more suitable. Tunable anisotropy and flexibility in device shape and size offer scalability and long term thermal stability desirable for applications.

J. Ryu, R. Thompson, S. Karube, N. Tezuka, M. Kohda, J. Nitta
Department of Materials Science
Tohoku University
Sendai 980–8579, Japan
E-mail: nitta@material.tohoku.ac.jp

C. O. Avci, M. Huang, G. S. D. Beach
Department of Materials Science and Engineering
Massachusetts Institute of Technology
Cambridge, MA 02139, USA

C. O. Avci
Institut de Ciència de Materials de Barcelona (ICMAB-CSIC)
Campus de la UAB
Bellaterra, Catalonia 08193, Spain

M. Song, J. Yang, S. Ko, K.-J. Kim
Department of Physics
Korea Advanced Institute of Science and Technology (KAIST)
Daejeon 34141, South Korea

M. Kohda, J. Nitta
Spintronics Research Network
Tohoku University
Sendai 980–8579, Japan

M. Kohda, J. Nitta
Organization for Advanced Studies
Center for Science and Innovation in Spintronics (Core Research Cluster)
Tohoku University
Sendai 980–8579, Japan

M. Kohda
Quantum Materials and Applications Research Center
National Institute for Quantum Science and Technology
1233 Watanuki, Takasaki, Gunma 370-1292, Japan

The ORCID identification number(s) for the author(s) of this article can be found under https://doi.org/10.1002/adfm.202209693

DOI: 10.1002/adfm.202209693

Moreover, SOT-induced switching has negligible incubation time since the magnetization and SOTs are orthogonal to each other, which ultimately results in ultrafast switching.[16,19–24] However, with **m** along **z**, the DL and FL-SOT effective fields have rotational and mirror symmetry relative to the *xz* and *xy* planes, respectively, which precludes switching by current alone. An in-plane field along **x** is necessary to break the rotational symmetry of the DL-SOT in a PMA magnet, which is the mechanism widely used in the vast majority of SOT switching experiments to date.[1,2,8,10,19,22]

In device applications, the external field can be applied locally by, e.g., stray fields from a nearby permanent magnet.[1,25] However, controlling stray fields in an integrated circuit that consists of nanometer-size devices is nontrivial and the additional magnetic elements increase the footprint of the final architecture. Therefore, a more practical local symmetry breaking mechanism is imperative. While important recent progress has been made,[26–52] significant challenges remain. For instance, ferromagnet/antiferromagnet bilayers have been used to induce an in-plane uniaxial exchange-bias field that can facilitate field-free deterministic switching,[27,38,46,47] but incomplete switching and thermal stability present challenges to device implementation. An alternative approach relies on generating spin currents with out-of-plane polarization (i.e., $\boldsymbol{\sigma} \parallel \pm \mathbf{z}$), for example by combining an interfacial spin galvanic effect and a spin precession mechanisms that leads to a unique current-dependent spin polarization symmetry.[48] Recent progresses also reveal the novel approach to break the symmetry, such as interlayer exchange coupling consisting of in-plane and out-of-plane ferromagnet layers,[47,53–55] single ferromagnet switching based on the low crystal symmetry property,[56,57] lateral spin-orbit torque induced by composition gradient or local laser annealing,[58,59] and ferromagnet/ferroelectric hybrid structures which generates the gradient spin current density.[60–62] However, all such mechanisms involve intricate multilayer structures,[49,50,60–62] shape and anisotropy engineering[40,42,44,51,52] and multiple inversion asymmetries[45,56,57] and/or complex physical phenomena.[27,38,46–48,53–55,58,59] If instead a symmetry-breaking mechanism could be engineered within the FM itself, device design and fabrication could be radically simplified, but so far this remains elusive.

Here we show that such symmetry breaking is readily present in epitaxial Co grown on Pt(111), giving rise to deterministic current-induced field-free switching in the most ubiquitous SOT material system. We find that such Co films with PMA possess a non-negligible in-plane (canted) magnetization component collinear with the current injection axis that acts to break the rotational symmetry of $\boldsymbol{\tau}_{DL}$. We furthermore reveal that the canted component arises from the local fluctuations of the thickness, hence the PMA, which drives relatively thicker Co (nanoscale) regions into a spin reorientation transition under the influence of a strong in-plane magnetocrystalline anisotropy. Through micromagnetic simulations, we find that the large Dzyaloshinkii-Moriya interaction (DMI) inherent to such systems couples the fully perpendicular and canted regions in a homochiral manner, which ultimately facilitates the field-free switching with pre-defined switching polarity for a given current direction. This finding offers the field-free switching approach that could be engineered at simpler material stacks, through local anisotropy engineering and exploiting the interplay of SOTs and DMI. We find that the field-free switching current density in epitaxial layers is slightly higher than that obtained from comparable polycrystalline Co/Pt layers in the presence of an external field, but significantly lower when normalized by the PMA or coercivity of the respective layers.

2. Results and Discussion

2.1. Crystal Structure and Magnetic Property in Epitaxial Co/Pt Bilayer

We deposited perpendicularly magnetized epitaxial AlO_x/Co(1 nm)/Pt(5 nm) layers by r.f. magnetron sputtering on MgO(111) and MgO(100) substrates, respectively (see Experimental Section and Section S1, Supporting Information). Polar x-ray diffraction (XRD) intensities show a clear 6-fold rotational symmetry for Co/Pt grown on MgO(111) (see **Figure 1**a, red data points), evidencing the high degree of epitaxy and excellent crystallinity. Co/Pt on MgO(100), on the other hand, shows 12-fold symmetry with a much lower intensity demonstrating the polycrystalline character (Figure 1a, blue data points). To confirm further the structural quality of Co/Pt we used high-resolution transmission electron microscopy to obtain cross sectional images with atomic resolution (Figure 1b,c; and Section S2, Supporting Information). Although Co and Pt cannot be distinguished from each other in these images, the coherent growth and single crystal structure of the Co/Pt bilayer on MgO(111) is evident from the real-space images and their Fourier transforms. A similar analysis of the Co/Pt on MgO(100) shows that the first few monolayers grow coherently with the (100) orientation of the MgO, whereas subsequent layers relax to a polycrystalline (111) texture. Hence Co and the Co/Pt interface is polycrystalline as also evidenced by the XRD polar scans in Figure 1a. Hence we refer below to Co/Pt(111) as the "epitaxial" sample and to Co/Pt(100) as the "polycrystalline" sample.

We prepared magnetic dots, 2 µm in diameter, at the intersection of a Pt Hall cross as depicted in Figure 1d (see Experimental Section). We measured the Hall resistance (R_H) that consists of anomalous Hall (R_A) and planar Hall (R_P) components defined as $R_H = R_A \cos\theta + R_P \sin 2\varphi \sin^2\theta$ (see Figure 1d for the definitions of φ and θ). Figure 1e shows R_H obtained by an out-of-plane ($\theta_B = 0°$) and in-plane magnetic field sweep ($\theta_B = 90°$) along the z and x directions, respectively, with a d.c. current of 1 mA (corresponding to $j = 0.83 \times 10^{11}\,\mathrm{A\,m^{-2}}$). Both samples show PMA with 100% remanence at $B_{ext} = 0$ mT although we observe substantial differences in the magnitude of R_H. The coercivity (B_c) of epitaxial Co/Pt is found to be ≈ 140 mT, which is 3.5 times larger than that of polycrystalline Co/Pt (≈ 40 mT). The effective anisotropy field (B_K) obtained using $B_K = B_{ext}(\sin\theta_B/\sin\theta - \cos\theta_B/\cos\theta)$ derived by macrospin approximation is extremely large in the epitaxial film ($B_K \approx 3.4$ T) compared to the polycrystalline Co/Pt ($B_K \approx 1.4$ T). We conclude that the PMA strongly depends on the crystallinity and the texture of these nominally identical Co/Pt layers grown on substrates terminated by two different crystal planes.

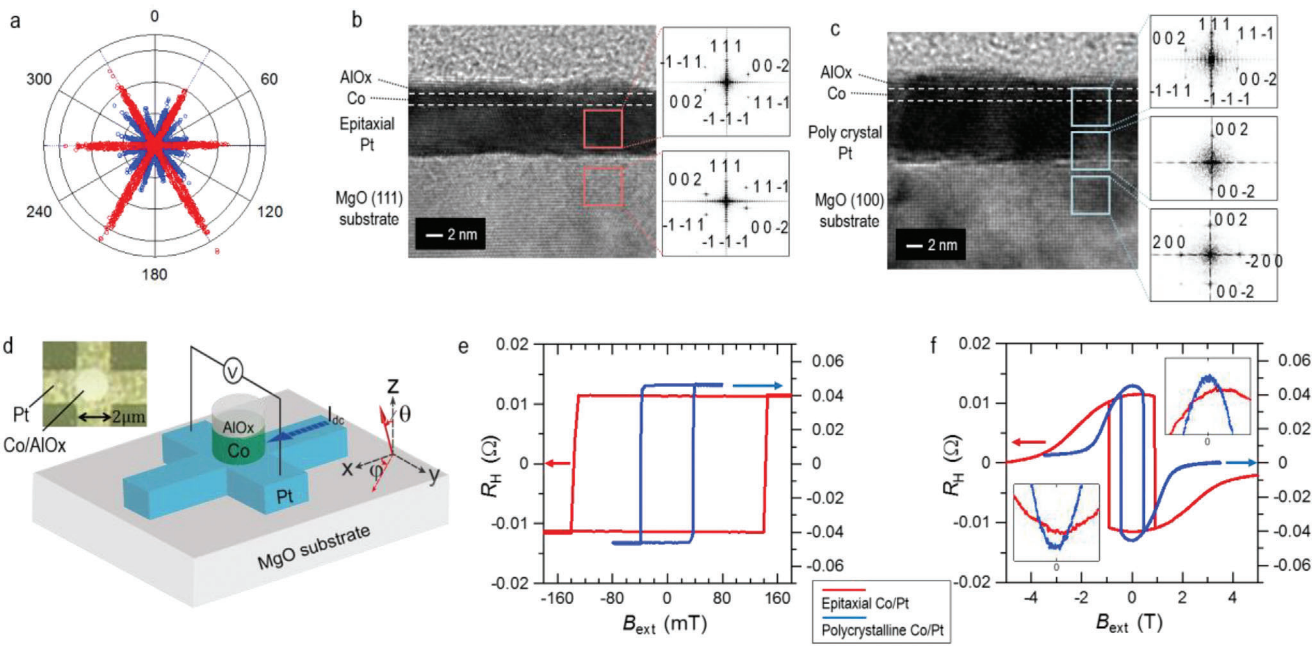

Figure 1. Characterization of crystal structure, device schematic and magnetic properties. a) In-plane X-ray diffraction data for epitaxial Co/Pt (red dots) and polycrystalline Co/Pt (blue dots). Each of the peaks obtained in epitaxial Co/Pt coincides with [110], [$\bar{1}$01], and [0$\bar{1}\bar{1}$], respectively. b,c) Cross sectional transmission electron micrographs for epitaxial Co/Pt b) and for polycrystalline Co/Pt c). Right panels in each figure show Fourier transforms of the region indicated by a box in the images. d) Schematics of electrical measurement on dot-shaped Hall device and its coordinate system. The inset shows microscopy image of a dot (Co/AlOx) and Hall cross (Pt). e) Hall resistance R_H as a function of applied field B_x applied along the out-of-plane direction ($\theta_B = 0°$). f) R_H with field applied along the in-plane direction ($\theta_B = 90°$) for epitaxial Co/Pt (red line) and polycrystalline Co/Pt (blue line). Insets in f) show the magnified results near zero magnetic field, revealing the asymmetry in R_H for epitaxial Co/Pt. In e) and f), the left and right axes correspond to the scale for epitaxial Co/Pt and polycrystalline Co/Pt, respectively.

2.2. Current-Induced Switching of Perpendicular Magnetization

To investigate SOT-driven magnetization reversal we swept a d.c. current in the presence and absence of an x-axis oriented external field B_x. In both the samples, we observe full and reversible switching above critical currents of the order of 15 mA (corresponding to $j = 1.25 \times 10^{12}$ A m^{-2}) with a moderate external field of $B_x = \pm 10$ mT, ± 80 mT for polycrystalline Co/Pt and epitaxial Co/Pt, respectively. The switching polarity inverts upon reversal of B_x, reflecting the expected DL-SOT symmetry. Note that the spin Hall angle obtained in our polycrystalline Co/Pt and epitaxial Co/Pt give 0.023 and 0.016, respectively, which show comparable magnitude with previous reports [63,64] (see Section S3, Supporting Information). Despite the large difference in the PMA and B_c of these two films, the critical current is only ≈20% higher in the case of epitaxial Co/Pt indicating substantially more efficient SOT in this film. Strikingly, in epitaxial Co/Pt, reversible switching is observed also in the absence of an external field, as depicted on the lower part of **Figure 2**a, with the same current density requirement as in the presence of B_x. This result cannot be understood in the framework of conventional SOT-induced switching and indicates that an additional mechanism is at play in the epitaxial layers.

To understand the above behavior, we investigated the field dependence of the switching in the two samples by applying a fixed current amplitude, set to a value larger than the critical value as determined in Figure 2a. The measurement consists of sequentially stepping the external field and then applying a fixed-polarity current pulse at each B_x, with m_z ($\propto R_H$) measured after each pulse injection. The results are depicted in Figure 2b. We observe that for the polycrystalline sample, the switching polarity inverts within a narrow field range of 10 mT centered symmetrically around $B_x = 0$, typical for SOT switching. However, in the epitaxial case, the sign reversal occurs across a broader field range and is shifted asymmetrically toward negative fields, evidencing an internal effective field that leads to deterministic switching at $B_x = 0$(see Section S4, Supporting Information for switching diagram).

To verify the robustness of this field-free switching phenomenon, we injected a train of pulses with equal amplitude, above the critical current, but with the polarity alternating randomly. The resulting switching sequence identically follows the current-pulse sequence verifying that switching is deterministic and not driven by thermal activation (Figure 2c). We measured over thirty devices fabricated from four different samples deposited at different times and nearly all of them showed deterministic switching (see Figure 2d). The switching polarity is predetermined by the local anisotropy fluctuations in the magnetic region as the detailed discussion would be followed in Section 2.3. Moreover, the switching is insensitive to application of moderate in-plane (along the y-axis up to 50 mT) and out-of-plane fields, showing that the mechanism is robust and relatively strong (see Section S5, Supporting Information).

In the absence of a symmetry breaking mechanism, field-free SOT switching of perpendicular magnetization can only occur if a current induces an out-of-plane field component that

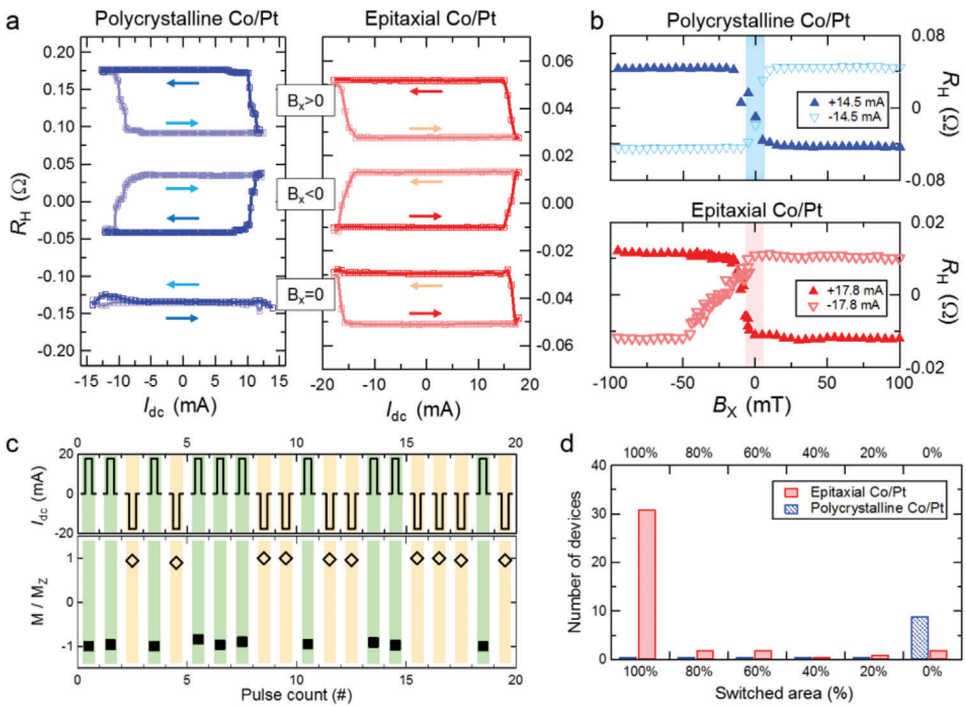

Figure 2. Magnetization switching as a function of external magnetic field. a) Current–induced magnetization switching depending on the sign of the applied field B_x. Left and right panels correspond to switching for polycrystalline Co/Pt (blue squares) and epitaxial Co/Pt (red squares), respectively. Note that $B_x = \pm$ 10mT and $B_x = \pm$ 80mT was applied for polycrystalline Co/Pt and epitaxial Co/Pt, respectively. Data are offset vertically for clarity. b) R_H measured after the injected pulsed current I_c as a function of B_x. Top and bottom panels correspond to polycrystalline Co/Pt and epitaxial Co/Pt samples, respectively Solid and open data points indicate positive and negative currents, respectively. The shaded regions indicate the field range where the change of switching polarity is expected to occur. c) Field free switching in epitaxial Co/Pt measured under current pulse injection. Top panel indicates the sequence of d.c. current pulses injected in the epitaxial Co/Pt sample in the absence of external fields. Bottom panel shows the magnetization state measured after current pulse application. d) Statistics on the number of devices for which field free magnetization switching was observed. Switched area indicates changes of R_H after current injection normalized by total R_H, such that 100% indicates full magnetization is observed in a given device, and values smaller than this indicate partial switching or no switching (0%). A total of 34 devices for epitaxial Co/Pt and 9 devices for polycrystalline Co/Pt were measured.

reverses its sign upon reversal of the current direction. Such an effect is known to exist in some non-centrosymmetric crystals with bulk inversion asymmetry, as in the recently reported WTe_2 semimetal structures.[65] However, the crystal structure of Co/Pt is centrosymmetric and such spin polarization is not expected. Instead, we find that the Hall resistance in the epitaxial samples is not symmetric with respect to $B_{x,y} = 0$. The data suggest there is an in-plane magnetization component biased along a fixed crystallographic direction, such that a compensating external field of the order of few tens of mT is required to achieve maximum R_H (see Figure 1f, inset; and Section S6, Supporting Information).

To characterize the in-plane magnetization component we measure Hall resistance by rotating the sample in the presence of a small in-plane field. In such measurements, for equilibrium magnetization pointing along the z-axis we expect a sin 2φ angular dependence due to the planar Hall effect (PHE), with an increasing amplitude as the field is increased, but with a decreasing offset as the z-component of the magnetization is diminishing due to tilting (**Figure 3**a – upper panel). This is exemplified in the polycrystalline sample as shown in Figure 3b – upper panel. However, in epitaxial layers the angular signal is significantly distorted due to the non-trivial (average) magnetization trajectory as depicted in Figure 3a – lower panel. A large and field-dependent cosine-like signal is superimposed on the expected sin 2φ signal, which can only be explained if the z-component of magnetization changes upon rotation. This set of measurements unequivocally shows that the magnetization has a non-negligible in-plane component in the epitaxial layers and may be contributing to the zero-field switching behavior observed in this sample as we discuss later.

Tilted magnetization is commonly observed in layers exhibiting a spin reorientation transition due to the competition between the PMA and in-plane and shape anisotropies.[66–70] However, very large (average) effective perpendicular anisotropy field calculated based on the Hall effect signal (>3 T) suggest that the spin reorientation transition is not a global property of the layers. Rather, we propose that local thickness variations of Co give rise to a spatial variation of PMA, and in some nanoscale regions with weaker PMA below the spin reorientation transition, the magnetization tends to tilt away from the z-axis (see Sections S6 and S7, Supporting Information). Evidence for this can be seen upon examination of the in-plane field sweep data as a function of φ_B, which exhibit butterfly-like loops superimposed to the expected symmetric AHE signal, reminiscent of the in-plane magnetization-originated PHE signal (see Section S6, Supporting Information). The jumps of this in-plane

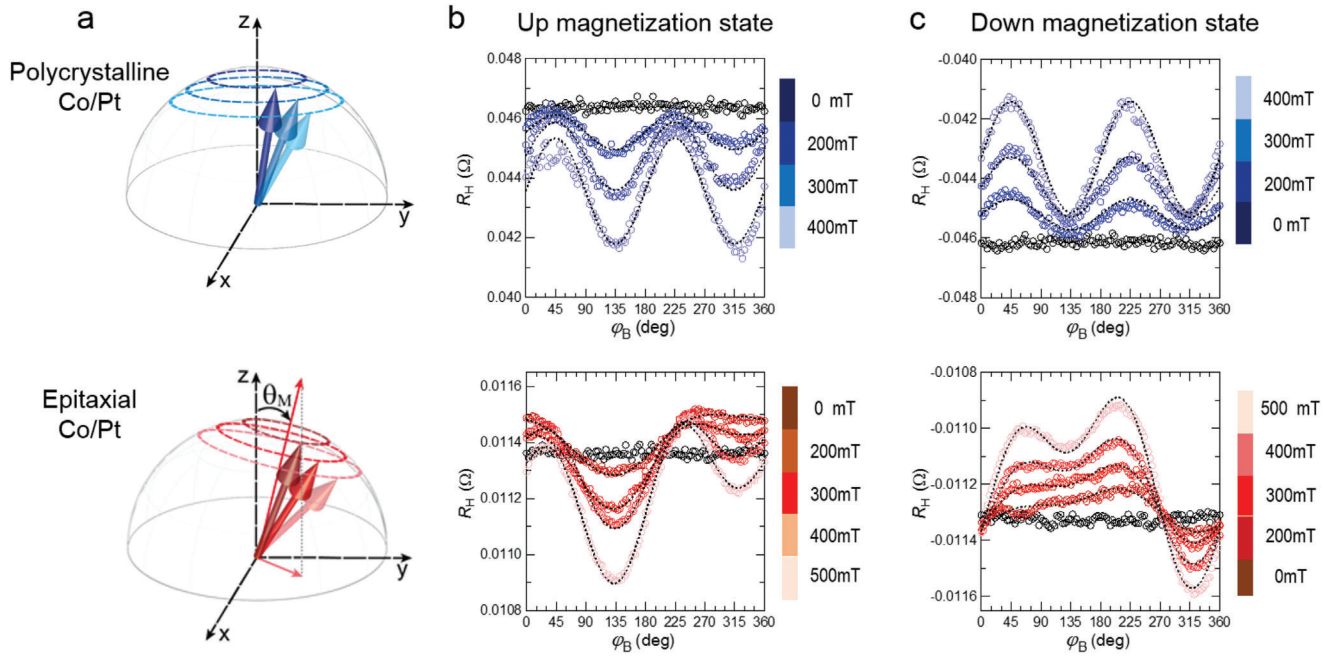

Figure 3. Azimuthal angle dependence of anomalous Hall effect (AHE). a) Illustrations showing the inferred behaviors of the magnetization orientation under in-plane field rotation for polycrystalline Co/Pt (top panel) and epitaxial Co/Pt (bottom panel). The magnetization in polycrystalline Co/Pt rotates around z-axis, however in epitaxial Co/Pt the average magnetization is tilted away from the z axis with an angle θ_M. Note that the arrows in a are one of the representative illustrations to describe the effect of the magnetization orientation under in-plane field rotation and the magnetization canting of each device might be randomly distributed over the devices. b,c) R_H as a function of azimuthal applied field angle φ_B in an initially up-magnetized state b) and down-magnetized state c). Black dotted lines are fits following $R_H = r_A \cos(\varphi_B - \varphi_c) + r_P \sin 2\varphi_B + \mathit{offset}$ where r_A and r_P are partial AHE and PHE contribution satisfying $0 < r_{A,P} < R_{A,P}$, and φ_c gives the canting angle with respect to the applied field angle. In the case of polycrystalline Co/Pt, R_H follows clear sin 2φ behavior with no apparent contribution from r_A. However, R_H in epitaxial Co/Pt is strongly affected by the canted magnetization giving rise to large r_A. For this sample we find $\varphi_c \sim 140 \pm 10°$. In a–c) top and bottom panels correspond to polycrystalline Co/Pt (blue dots) and epitaxial Co/Pt (red dots), respectively.

signal reflecting the switching of the in-plane magnetization coincide with that of the out-of-plane magnetization reversal. This shows that the switching of the in-plane and out-of-plane components are coupled and this coupling must be chiral due to the strong interfacial DMI inherent to the Co/Pt system,[71,72] which are estimated as ≈2.0 mJ m^{-2} in polycrystalline Co/Pt and ≈2.3 mJ m^{-2} in epitaxial Co/Pt, that fixes the chirality of nonuniform magnetization textures[35,36] (see Section S3, Supporting Information). Indeed, simultaneous switching of chirally-coupled nanomagnets in engineered devices made of Pt/Co has been recently demonstrated.[35,36]

2.3. Micromagnetic Simulation in the Presence of Canted Anisotropy

In **Figure 4** we present comprehensive micromagnetic simulations to test the above hypothesis and the different conditions that may lead to field-free switching in the presence of canted nanoscale regions in the Co dot.[73] First, we start with a circular dot 500 nm in diameter possessing uniform PMA. Injecting current pulses of $j = 3 \times 10^{12}$ A m^{-2} well above the switching threshold does not lead to any switching behavior (Figure 4a), as expected. Then, we introduce a boundary region with reduced anisotropy, which is usually the case in lithographically defined dots. Note that the edges of the dot will be naturally canted due to the DMI (see Ref. [23]). Again, no switching behavior is observed under these conditions (Figure 4b). Next, we introduce randomly distributed relatively large regions with reduced PMA, such that the magnetization within these regions is slightly tilted in-plane, and we omit the boundary region. Once more, the switching is not observed (Figure 4c). Next, we include the boundary region as well as the randomly distributed local anisotropy fluctuations (canted regions), which makes the simulation closer to the real situation in our devices. Surprisingly, the switching of the entire dot is achieved in a deterministic manner (Figure 4d). We then test the same condition with smaller regions of canted magnetization, and again observe 100% deterministic switching (Figure 4e). Lastly, we tested the role of the DMI and performed the simulations corresponding to the situation in Figure 4e but setting the DMI to zero. Strikingly, the switching did not occur in this case (Figure 4f), showing the essential role of the DMI in magnetically coupling the regions with different PMA in a chiral manner. These simulations combined with our experimental demonstration unequivocally show that the combination of the canted magnetization at the edge of the magnetic dot, the local anisotropy fluctuations, and the DMI lead to deterministic field-free switching in the Co/Pt epitaxial system. Moreover, we find that only the small region of the reduced magnetic anisotropy formed at the edge could break the symmetry and generate the field-free switching (see Section S8, Supporting Information).

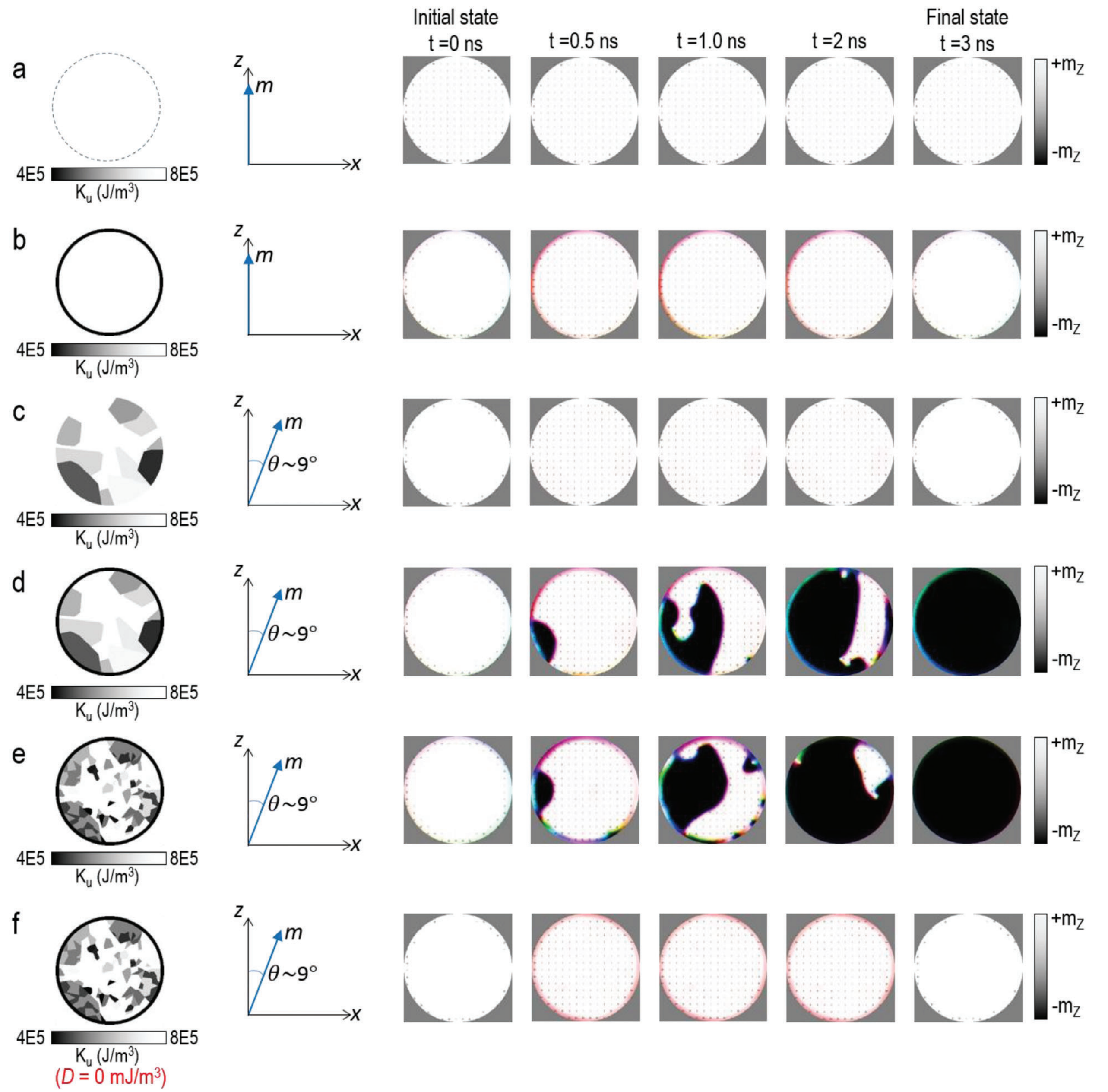

Figure 4. Micromagnetic simulation of field-free switching. a) Co dot which owns uniform PMA without boundary. b) The defined Co dot with the uniform PMA. c) Co dot with the tilted magnetization induced by local anisotropy distribution without boundary. In a–c), the magnetization switching is not obtained without the external magnetic field. d) The defined Co dot with the tilted magnetization. e) The defined Co dot where a smaller scale of anisotropy distribution exists. In d) and e), deterministic switching is achieved. f) Co dot which has the tilted magnetization as the same condition of case c but in the absence of DMI. In a–f), The first and second column shows the boundary region of Co dot with a 500 nm diameter in the presence of local anisotropy fluctuations and the canted state of Co dot due to the anisotropy fluctuations, respectively. Here θ_M represents the polar angle of magnetization. The color bar below the Co dot indicates the distribution of perpendicular magnetic anisotropy parameter K_u. Here the DMI energy density for cases a–e) is set as 1.0 mJ m^{-3} except for the case f) which represents the absence of DMI. The third row represents a time-dependent snapshot of magnetization switching in micro-magnetic simulations.

The above results are highly appealing from a technological application perspective. The successful switching in the simulated dots with small and large grain size indicates that the dot size can be significantly downscaled, which would be required in applications such as in the SOT-operated magnetic random access memories. Indeed, we tested the feasibility of varying the deposition conditions in an attempt to vary the grain size. We observed the switching behavior in epitaxial Co/Pt at higher growth temperature (≈400 °C) which should result in a different grain size with respect to the layers grown at 200 °C reported above (see Section S9, Supporting Information). Therefore, we anticipate that with a more systematic engineering effort, which goes beyond the scope of this study, small devices with suitable spintronic properties and field-free switching behavior can be fabricated. Moreover, the top oxide layer AlO_x used here can be substituted with MgO (a more suitable oxide barrier for tunnel junction devices) without significantly affecting the switching behavior. We note that the local thickness fluctuation could not be favored to achieve the high tunnel magneto resistance (TMR). However, further artificial material/device engineering approaches could overcome this issue. For example, the condition that the edge could be artificially engineered to have lower anisotropy enables field-free switching without producing the local thickness fluctuation[36] (see Section S8, Supporting Information). From the practical point of view, two alternative methods could be implemented to further increase the reliability of controlling the certain preferential canting direction. The first one relies on an in-plane field application during the deposition of Co. This helps quench the canting direction, and hence set the switching polarity deterministically. Combining these approaches with the degree of freedom offered by the growth temperature tuning and post-growth annealing, the thickness fluctuations mediated canting can be possibly engineered to have a deterministic angle and direction. The second approach suggests that local anisotropy control of certain device regions as we provide the simulation results in Section S8 (Supporting Information). This post-growth control of local anisotropy could be obtained by, e.g., focused ion bombardment ,[74,75] and further can provide a universal recipe for the systems characterized by strong the SOTs and interfacial DMI, not limited to Pt/Co bilayers. Finally, we note that, so far, the majority of published SOT studies has considered polycrystalline Co/Pt layers that shows rather a uniform PMA throughout the layers. However, our results indicate that epitaxial layers offer further versatility and additional degrees of freedom for tuning the material properties for SOT switching applications that could be beneficial for future spintronic devices.

3. Conclusion

In summary, we observe deterministic current-induced switching of perpendicularly magnetized epitaxial Co/Pt(111) bilayers in the absence of an external magnetic field. We find that the in-plane field requirement is lifted in epitaxial layers due to the non-negligible in-plane component of magnetization, breaking the rotational symmetry of damping-like torque responsible for switching. Measurements suggest that, despite the large average perpendicular magnetic anisotropy, there exist nanoscale regions with magnetization tilted off the perpendicular axis due to the competition between the out-of-plane and in-plane anisotropies. We argue, and support with micromagnetic simulations, that the interplay between the strong DMI and local regions with easy-plane anisotropy couples the out-of-plane regions with the in-plane canted regions in such a manner that reversible, deterministic switching can be obtained without any external field. This simple and effective method to achieve external field-free switching in the archetypal Co/Pt structure will be highly beneficial to develop, e.g., SOT-operated magnetic random-access memories. Furthermore, our findings will stimulate further research to exploit anisotropy engineering in thin film magnetic heterostructures.

4. Experimental Section

Material Growth and Characterization: Perpendicularly magnetized Co/Pt films were deposited on MgO (100) and MgO (111) substrates, by r.f. magnetron sputtering with a base pressure of 8×10^{-7} Pa. During Pt deposition the substrate was heated to 200 °C to ensure epitaxial growth following the orientation of MgO substrate. Co layers were then deposited after cooling the substrate to room temperature. All films were capped with AlOx (2.0 nm) by sputtering in situ Al_2O_3 target.

Crystallographic characterization of the films was performed by x-ray diffraction for both out-of-plane (see Section S1, Supporting Information) and in-plane beam incidence, as well as by real-space atomic-resolution imaging using cross sectional transmission electron microscopy. Magneto optical Kerr effect was used to investigate magnetic properties of the continuous films before device fabrication.

Device Fabrication: The deposited Co (1.0 nm)/Pt (5.0 nm) films were patterned using electron beam lithography. First, Co/Pt dots with 2 µm diameter were defined by Ar^+ milling, with endpoint detection used to stop the etch at the Co/Pt interface. Hall bar arms with 2 µm width and 10 µm(length) were then patterned by a subsequent lithography step followed by Ar^+ milling through the remaining Pt layer. Finally, contact pads of Ta (3.0 nm)/Au (80 nm) were deposited by electron beam evaporation followed by lift-off.

Electrical Measurements: Current-induced switching measurement were performed using a sourcemeter for current injection and a voltmeter for Hall voltage acquisition. The injected current pulses for switching measurements were 30 ms long. Azimuthal angle dependence of Hall resistance in Figure 3 was measured by lock-in amplifier.

Micromagnetic Simulations: Micromagnetic simulations using MuMax3 software,[73] based on Landau-Lifshitz-Gilbert (LLG) equation with SOTs term were performed to investigate the magnetization dynamics during the switching process. The diameter and thickness of the Co dot are 500 and 1 nm, respectively. A simulation cell size is 2 nm × 2 nm × 1 nm, and all simulations were carried out at zero temperature. Material parameters were following Co/Pt system: saturation magnetization $M_s = 5.8 \times 10^5$ A m^{-1}, exchange stiffness $A = 1.5 \times 10^{-11}$ J m^{-1}, damping constant $\alpha = 0.3$, and spin Hall angle $\theta_{SH} = 0.1$. The interfacial DMI constant was set to $D = 1.0 \times 10^{-3}$ J m^{-2} except for the case of Figure 4f. A uniaxial anisotropy constant K_u had a grain-wise spatial variation, as shown in Figure 4. Specifically, the boundary region with reduced anisotropy (15-nm-wide black ring shown in Figure 4b,d–f), had a uniform $K_u = 2.0 \times 10^5$ J m^{-3}. At the relatively large regions with reduced PMA (Figure 4c–f), the anisotropy constant K_u follows a Gaussian distribution centered at 5.0×10^5 J m^{-3} with a standard deviation of 1.0×10^5 J m^{-3}. For the smaller grains (Figure 4e, f), K_u follows the same Gaussian distribution (inside the relatively large regions), or an exponential distribution (outside the relatively large regions) with an upper limit of 8.0×10^5 J m^{-3} and decaying constant of 1.0×10^5 J m^{-3}. The simulated current density was $j = 3 \times 10^{12}$ A m^{-2}. The polar angle θ_M representing the magnetization tilting was estimated by a z-component magnitude of total magnetization of the entire Co dot. All simulations were carried out at zero external field.

Supporting Information

Supporting Information is available from the Wiley Online Library or from the author.

Acknowledgements

J.R. and C.O.A. contributed equally to this work. This work was supported by the Japan Society for the Promotion of Science with Grant-in-Aid 15H05699, 25220604, 15H02099, 25220604 and 15H05854. Work at MIT was supported by the US Department of Energy, Office of Science, Basic Energy Sciences under Award no. DE-SC0012371. K-J. K. acknowledge the support by KAIST-funded Global Singularity Research Program for 2021.

The authors acknowledge technical support from Dr. David Bono, Dr. Keita Nakagawara, Dr. Maxwell Mann, and Dr. Takamichi Miyazaki.

Conflict of Interest

The authors declare no conflict of interest.

Data Availability Statement

The data that support the findings of this study are available from the corresponding author upon reasonable request.

Keywords

deterministic switching, epitaxial Co/Pt, field-free switching, spin-orbit torques

Received: August 21, 2022
Revised: April 23, 2023
Published online:

[1] I. M. Miron, K. Garello, G. Gaudin, P.-J. Zermatten, M. V. Costache, S. Auffret, S. Bandiera, B. Rodmacq, A. Schuhl, P. Gambardella, *Nature* **2011**, *476*, 189.
[2] L. Liu, C. F. Pai, Y. Li, H. W. Tseng, D. C. Ralph, R. A. Buhrman, *Science* **2012**, *336*, 555.
[3] K. Garello, I. M. Miron, C. O. Avci, F. Freimuth, Y. Mokrousov, S. Blügel, S. Auffret, O. Boulle, G. Gaudin, P. Gambardella, *Nat. Nanotechnol.* **2013**, *8*, 587.
[4] J. Kim, J. Sinha, M. Hayashi, M. Yamanouchi, S. Fukami, T. Suzuki, S. Mitani, H. Ohno, *Nat. Mater.* **2013**, *12*, 240.
[5] S. Emori, U. Bauer, S. M. Ahn, E. Martinez, G. S. D. Beach, *Nat. Mater.* **2013**, *12*, 611.
[6] K. Ryu, L. Thomas, S. Yang, S. Parkin, *Nat. Nanotechnol.* **2013**, *8*, 527.
[7] P. P. J. Haazen, E. Murè, J. H. Franken, R. Lavrijsen, H. J. M. Swagten, B. Koopmans, *Nat. Mater.* **2013**, *12*, 299.
[8] C. O. Avci, A. Quindeau, C.-F. Pai, M. Mann, L. Caretta, A. S. Tang, M. C. Onbasli, C. A. Ross, G. S. D. Beach, *Nat. Mater.* **2017**, *16*, 309.
[9] X. Fan, J. Wu, Y. Chen, M. J. Jerry, H. Zhang, J. Q. Xiao, *Nat. Commun.* **2013**, *4*, 1799.
[10] O. J. Lee, L. Q. Liu, C. F. Pai, Y. Li, H. W. Tseng, P. G. Gowtham, J. P. Park, D. C. Ralph, R. A. Buhrman, *Phys. Rev. B* **2014**, *89*, 024418.
[11] C. F. Pai, L. Liu, Y. Li, H. W. Tseng, D. C. Ralph, R. A. Buhrman, *Appl. Phys. Lett.* **2012**, *101*, 122404.
[12] Z. Diao, Z. Li, S. Wang, Y. Ding, A. Panchula, E. Chen, L. C. Wang, Y. Huai, *J. Phys.: Condens. Matter* **2007**, *19*, 165209.
[13] S. Ikeda, K. Miura, H. Yamamoto, K. Mizunuma, H. D. Gan, M. Endo, S. Kanai, J. Hayakawa, F. Matsukura, H. Ohno, *Nat. Mater.* **2010**, *9*, 721.
[14] M. Cubukcu, O. Boulle, M. Drouard, K. Garello, C. O. Avci, I. M. Miron, J. Langer, B. Ocker, P. Gambardella, G. Gaudin, *Appl. Phys. Lett.* **2014**, *104*, 042406.
[15] M. Yamanouchi, L. Chen, J. Kim, M. Hayashi, H. Sato, S. Fukami, S. Ikeda, F. Matsukura, H. Ohno, *Appl. Phys. Lett.* **2013**, *102*, 212408.
[16] V. Krizakova, K. Garello, E. Grimaldi, G. S. Kar, P. Gambardella, *Appl. Phys. Lett.* **2020**, *116*, 232406.
[17] C. O. Avci, G. S. D. Beach, P. Gambardella, *Phys. Rev. B* **2019**, *100*, 235454.
[18] T. Devolder, J. Hayakawa, K. Ito, H. Takahashi, S. Ikeda, P. Crozat, N. Zerounian, J. Von Kim, C. Chappert, H. Ohno, *Phys. Rev. Lett.* **2008**, *100*, 057206.
[19] K. Garello, C. O. Avci, I. M. Miron, M. Baumgartner, A. Ghosh, S. Auffret, O. Boulle, G. Gaudin, P. Gambardella, *Appl. Phys. Lett.* **2014**, *105*, 212402.
[20] C. Zhang, S. Fukami, H. Sato, F. Matsukura, H. Ohno, *Appl. Phys. Lett.* **2015**, *107*, 012401.
[21] C. O. Avci, E. Rosenberg, M. Baumgartner, L. Beran, A. Quindeau, P. Gambardella, C. A. Ross, G. S. D. Beach, *Appl. Phys. Lett.* **2017**, *111*, 072406.
[22] M. Baumgartner, K. Garello, J. Mendil, C. O. Avci, E. Grimaldi, C. Murer, J. Feng, M. Gabureac, C. Stamm, Y. Acremann, S. Finizio, S. Wintz, J. Raabe, P. Gambardella, *Nat. Nanotechnol.* **2017**, *12*, 980.
[23] C. Donnelly, S. Finizio, S. Gliga, M. Holler, A. Hrabec, M. Odstrčil, S. Mayr, V. Scagnoli, L. J. Heyderman, M. Guizar-Sicairos, J. Raabe, *Nat. Nanotechnol.* **2020**, *15*, 356.
[24] E. Grimaldi, V. Krizakova, G. Sala, F. Yasin, S. Couet, G. Sankar Kar, K. Garello, P. Gambardella, *Nat. Nanotechnol.* **2020**, *15*, 111.
[25] K. Garello, F. Yasin, H. Hody, S. Couet, L. Souriau, S. H. Sharifi, J. Swerts, R. Carpenter, S. Rao, W. Kim, J. Wu, K. K. V. Sethu, M. Pak, N. Jossart, D. Crotti, A. Furnémont, G. S. Kar, presented at *2019 Symp. VLSI Circuits*, Kyoto, Japan, June **2019**.
[26] G. Yu, P. Upadhyaya, Y. Fan, J. G. Alzate, W. Jiang, K. L. Wong, S. Takei, S. A. Bender, L. Chang, Y. Jiang, M. Lang, J. Tang, Y. Wang, Y. Tserkovnyak, P. K. Amiri, K. L. Wang, *Nat. Nanotechnol.* **2014**, *9*, 548.
[27] S. Fukami, C. Zhang, S. Duttagupta, A. Kurenkov, H. Ohno, *Nat. Mater.* **2016**, *15*, 535.
[28] J. M. Lee, K. Cai, G. Yang, Y. Liu, R. Ramaswamy, P. He, H. Yang, *Nano Lett.* **2018**, *18*, 4669.
[29] B. Chen, J. Lourembam, G. Sarjoosing, S. T. Lim, *Appl. Phys. Lett.* **2018**, *114*, 022401.
[30] B. Cui, D. Li, J. Yun, Y. Zuo, X. Guo, K. Wu, X. Zhang, Y. Wang, L. Xi, D. Xue, *Phys. Chem. Chem. Phys.* **2018**, *20*, 9904.
[31] Y. Liu, B. Zhou, J.-G. Zhu, *Sci. Rep.* **2018**, *9*, 325.
[32] X. Li, A. Kang, Z. Liu, Y. Zhou, *Appl. Phys. Lett.* **2019**, *114*, 012403.
[33] M. Wang, W. Cai, D. Zhu, Z. Wang, J. Kan, Z. Zhao, K. Cao, Z. Wang, Y. Zhang, T. Zhang, C. Park, J. P. Wang, A. Fert, W. Zhao, *Nat. Electron.* **2018**, *1*, 582.
[34] T. Y. Chen, H. I. Chan, W. B. Liao, C. F. Pai, *Phys. Rev. Appl.* **2018**, *10*, 044038.
[35] Z. Luo, T. P. Dao, A. Hrabec, J. Vijayakumar, A. Kleibert, M. Baumgartner, E. Kirk, J. Cui, T. Savchenko, G. Krishnaswamy, L. J. Heyderman, P. Gambardella, *Science* **2019**, *363*, 1435.
[36] T. P. Dao, M. Müller, Z. Luo, M. Baumgartner, A. Hrabec, L. J. Heyderman, P. Gambardella, *Nano Lett.* **2019**, *19*, 5930.
[37] J. Ryu, S. Lee, K.-J. Lee, B.-G. Park, *Adv. Mater.* **2020**, *32*, 1907148.
[38] A. van den Brink, G. Vermijs, A. Solignac, J. Koo, J. T. Kohlhepp, H. J. M. Swagten, B. Koopmans, *Nat. Commun.* **2016**, *7*, 10854.
[39] Q. Shao, P. Li, L. Liu, H. Yang, S. Fukami, A. Razavi, H. Wu, K. Wang, F. Freimuth, Y. Mokrousov, M. D. Stiles, S. Emori, A. Hoffmann, J. Akerman, K. Roy, J. P. Wang, S. H. Yang, K. Garello, W. Zhang, *IEEE Trans. Magn.* **2021**, *57*, 800439.
[40] Z. Zheng, Y. Zhang, V. Lopez-Dominguez, L. Sánchez-Tejerina, J. Shi, X. Feng, L. Chen, Z. Wang, Z. Zhang, K. Zhang, B. Hong, Y. Xu, Y. Zhang, M. Carpentieri, A. Fert, G. Finocchio, W. Zhao, P. K. Amiri, *Nat. Commun.* **2021**, *12*, 4555.
[41] M. G. Kang, J. G. Choi, J. Jeong, J. Y. Park, H. J. Park, T. Kim, T. Lee, K. J. Kim, K. W. Kim, J. H. Oh, D. D. Viet, J. R. Jeong, J. M. Yuk, J. Park, K. J. Lee, B. G. Park, *Nat. Commun.* **2021**, *12*, 7111.
[42] H. Wu, J. Nance, S. A. Razavi, D. Lujan, B. Dai, Y. Liu, H. He, B. Cui, D. Wu, K. Wong, K. Sobotkiewich, X. Li, G. P. Carman, K. L. Wang, *Nano Lett.* **2021**, *21*, 515.
[43] J. Ryu, R. Thompson, J. Y. Park, S.-J. Kim, G. Choi, J. Kang, H. B. Jeong, M. Kohda, J. M. Yuk, J. Nitta, K.-J. Lee, B.-G. Park, *Nat. Electron.* **2022**, *5*, 217.

[44] H. J. Kim, K. W. Moon, B. X. Tran, S. Yoon, C. Kim, S. Yang, J. H. Ha, K. An, T. S. Ju, J. Il Hong, C. Hwang, *Adv. Funct. Mater.* **2022**, *32*, 2112561.
[45] Q. Huang, C. Guan, Y. Fan, X. Zhao, X. Han, Y. Dong, X. Xie, T. Zhou, L. Bai, Y. Peng, Y. Tian, S. Yan, *ACS Nano* **2022**, *16*, 12462.
[46] Y.-W. Oh, S. C. Baek, Y. M. Kim, H.-Y. Lee, K.-D. Lee, C.-G. Yang, E.-S. Park, K.-S. Lee, K.-W. Kim, G. Go, J.-R. Jeong, B.-C. Min, H.-W. Lee, K.-J. Lee, B.-G. Park, *Nat. Nanotechnol.* **2016**, *11*, 878.
[47] Y. C. Lau, D. Betto, K. Rode, J. M. D. Coey, P. Stamenov, *Nat. Nanotechnol.* **2016**, *11*, 758.
[48] S. C. Baek, V. P. Amin, Y.-W. Oh, G. Go, S.-J. Lee, G.-H. Lee, K.-J. Kim, M. D. Stiles, B.-G. Park, K.-J. Lee, *Nat. Mater.* **2018**, *17*, 509.
[49] Q. Ma, Y. Li, D. B. Gopman, Y. P. Kabanov, R. D. Shull, C. L. Chien, *Phys. Rev. Lett.* **2018**, *120*, 117703.
[50] N. Sato, F. Xue, R. M. White, C. Bi, S. X. Wang, *Nat. Electron.* **2018**, *1*, 508.
[51] C. K. Safeer, E. Jué, A. Lopez, L. Buda-Prejbeanu, S. Auffret, S. Pizzini, O. Boulle, I. M. Miron, G. Gaudin, *Nat. Nanotechnol.* **2016**, *11*, 143.
[52] M. Kazemi, G. E. Rowlands, S. Shi, R. A. Buhrman, E. G. Friedman, *IEEE Trans. Electron Devices* **2016**, *63*, 4499.
[53] W. Y. Kwak, J. H. Kwon, P. Grünberg, S. H. Han, B. K. Cho, *Sci. Rep.* **2018**, *8*, 3826.
[54] Y. Sheng, K. W. Edmonds, X. Ma, H. Zheng, K. Wang, *Adv. Electron. Mater.* **2018**, *4*, 1800224.
[55] J. Wei, X. Wang, B. Cui, C. Guo, H. Xu, Y. Guang, Y. Wang, X. Luo, C. Wan, J. Feng, H. Wei, G. Yin, X. Han, G. Yu, *Adv. Funct. Mater.* **2022**, *32*, 2109455.
[56] L. Liu, C. Zhou, X. Shu, C. Li, T. Zhao, W. Lin, J. Deng, Q. Xie, S. Chen, J. Zhou, R. Guo, H. Wang, J. Yu, S. Shi, P. Yang, S. Pennycook, A. Manchon, J. Chen, *Nat. Nanotechnol.* **2021**, *16*, 277.
[57] L. Liu, C. Zhou, T. Zhao, B. Yao, J. Zhou, X. Shu, S. Chen, S. Shi, S. Xi, D. Lan, W. Lin, Q. Xie, L. Ren, Z. Luo, C. Sun, P. Yang, E. J. Guo, Z. Dong, A. Manchon, J. Chen, *Nat. Commun.* **2022**, *13*, 3539.
[58] Y. Cao, Y. Sheng, K. W. Edmonds, Y. Ji, H. Zheng, K. Wang, *Adv. Mater.* **2020**, *32*, 1907929.
[59] X. Shu, L. Liu, J. Zhou, W. Lin, Q. Xie, T. Zhao, C. Zhou, S. Chen, H. Wang, J. Chai, Y. Ding, W. Chen, J. Chen, *Phys. Rev. Appl.* **2022**, *17*, 024031.
[60] K. Cai, M. Yang, H. Ju, S. Wang, Y. Ji, B. Li, K. W. Edmonds, Y. Sheng, B. Zhang, N. Zhang, S. Liu, H. Zheng, K. Wang, *Nat. Mater.* **2017**, *16*, 712.
[61] M. Yang, J. Luo, Y. Ji, H.-Z. Zheng, K. Wang, Y. Deng, Z. Wu, K. Cai, K. W. Edmonds, Y. Li, Y. Sheng, S. Wang, Y. Cui, *IEEE Electron Device Lett.* **2019**, *40*, 1554.
[62] R. Li, Y. Li, Y. Sheng, Z. A. Bekele, K. Wang, *ACS Appl. Electron. Mater.* **2021**, *3*, 2646.
[63] J. Ryu, C. O. Avci, S. Karube, M. Kohda, G. S. D. Beach, J. Nitta, *Appl. Phys. Lett.* **2019**, *114*, 142402.
[64] Q. Bai, J. Mao, J. Yun, Y. Zhai, M. Chang, X. Zhang, J. Zhang, Y. Zuo, L. Xi, *Appl. Phys. Lett.* **2021**, *118*, 132403.
[65] D. MacNeill, G. M. Stiehl, M. H. D. Guimaraes, R. A. Buhrman, J. Park, D. C. Ralph, *Nat. Phys.* **2017**, *13*, 300.
[66] K. D. Usadel, A. Hucht, *Phys. Rev. B* **2002**, *66*, 244191.
[67] R. Frömter, H. Stillrich, C. Menk, H. P. Oepen, *Phys. Rev. Lett.* **2008**, *100*, 207202.
[68] R. L. Stamps, L. Louail, M. Hehn, M. Gester, K. Ounadjela, *J. Appl. Phys.* **1997**, *81*, 4751.
[69] J. W. Lee, J. R. Jeong, S. C. Shin, J. Kim, S. K. Kim, *Phys. Rev. B* **2002**, *66*, 172404.
[70] H. Stillrich, C. Menk, R. Frömter, H. P. Oepen, *J. Appl. Phys.* **2009**, *105*, 07C308.
[71] A. Hrabec, N. A. Porter, A. Wells, M. J. Benitez, G. Burnell, S. Mcvitie, D. Mcgrouther, T. A. Moore, C. H. Marrows, *Phys. Rev. B* **2014**, *90*, 020402(R).
[72] E. C. Corredor, S. Kuhrau, F. Kloodt-Twesten, R. Frömter, H. P. Oepen, *Phys. Rev. B* **2017**, *96*, 060410(R).
[73] A. Vansteenkiste, J. Leliaert, M. Dvornik, M. Helsen, F. Garcia-Sanchez, B. Van Waeyenberge, *AIP Adv.* **2014**, *4*, 107133.
[74] D. Engel, A. Kronenberger, M. Jung, H. Schmoranzer, A. Ehresmann, A. Paetzold, K. Röll, *J. Magn. Magn. Mater.* **2003**, *263*, 275.
[75] M. Matczak, B. Szymański, P. Kuświk, M. Urbaniak, F. Stobiecki, Z. Kurant, A. Maziewski, D. Lengemann, A. Ehresmann, *Nanoscale Res. Lett.* **2014**, *9*, 395.